Osteoformation potential of an allogenic partially demineralized bone matrix in critical-size defects in the rat calvarium

Ahmad Moustapha Diallo, Ahmad Moustapha Diallo, Solène Rota, Michel Boissière, Raphaël Bardonnet, Emmanuel Pauthe, Hervé Petite, Henri M Benoist, Morad Bensidhoum, Fani Anagnostou

Osteoformation potential of an allogenic partially demineralized bone matrix in critical-size defects in the rat calvarium

Running Title: Injectable allograft promotes calvarial-defects bone regeneration

Ahmad Moustapha Diallo[a,b], Solène Rota[c,d], Michel Boissière[c], Raphaël Bardonnet[d], Emmanuel Pauthe[c], Hervé Petite[a], Henri M. Benoist[b], Morad Bensidhoum[a], Fani Anagnostou[a,e*]

a. CNRS UMR 7052 - INSERM U1271, Laboratory of Osteoarticular Biology, Bioengineering and Bioimaging, Universiy of Paris, 10 Avenue de Verdun, 75010 Paris, France.
b. Service of Periodontology, Institute of Odontology and Stomatology (IOS); Faculty of Medecine, Pharmacy and Odonto-Stomatology; University Cheikh Anta Diop (UCAD) BP 5005 Dakar-Fann, Sénégal.
c. ERRMECe, Research Team on Extracellular Matrix-Cellular Relationships (EA1391), Biomaterials for Health Research Group, Institute of Materials I-MAT (FD4122), CY Tech, CY University Cergy Paris, International House of Research (MIR), rue Descartes, 95001 Neuville sur Oise cedex, France.
d. Biobank, 3 rue Georges Charpak 77127 Lieusaint, France,
e. Service of Odontology, Hôpital Pitié-Salpêtrière APHP, U.F.R. of Odontology University of Paris, 47-83 Boulevard de l'Hôpital, 75013 Paris, France

*** Corresponding author: fani.anagnostou@univ-paris-diderot.fr; Tel.: +33-(0)1-57-27-85-70**

ABSTRACT

Allogenic demineralized bone matrix has been developed as a reliable alternative to the autologous bone graft. In the present study, we assessed the osteoformation potential of a partially demineralized bone matrix (PDBM) in a paste form obtained without an added carrier. This formulation included the preparation of cancelous bone from femoral heads after decellularision, delipidation, demineralization in HCl and autoclaving at 121°C. Structural and biochemical characteristics of PDBM were determined using FTIR (Fourier transform infrared spectroscopy), hydroxyproline, DNA content assays, and optical ellipsometry. The osteoformation potential was evaluated in 8-, 6-, and 4-mm-diameter rat-calvarial bone defects by *in vivo* micro-CT analysis, performed immediately after surgery on days 0, 15, 30, 45, and 60. Moreover, histological and histomorphometric analyses were done on day 60. PDBM was compared to cancelous bone powder (BP) before its partial demineralization. The expression levels of selected inflammation-, angiogenesis-, and bone-related genes were also investigated by RT-PCR, 3, 7, and 14 days after surgery.Compared to the control group, the PDBM group exhibited a significant increase ($p<0.05$) in radiopacity in 8-mm- and 6-mm-diameter defects at all time points tested. On day 60, the amount of newly-formed bone was greater (16 and 1.6 folds; $p<0.001$; respectively) compared to that in control defects. No bone formation was observed in defects filled with BP regardeless of the size. In 8-mm-diameter defect, PDBM was effective enough to induce the upregulation of genes pertinent to inflammation (i.e., TNFα, IL-6, and IL-8), angiogenesis (i.e., VEGF, VWF), and osteogenesis (ALP, RUNX2, BGLAP, SP7) by day 3 after surgery.This study showed that the tested PDBM deeply influences the early critical events involved in bone regeneration and exhibits efficient osteoformation capacity, making it an attractive graft option for treating defects in periodontal and maxillofacial areas.

Keywords: critical-size bone defect; bone regeneration; calvarial defect; demineralized bone matrix; bone allograft

1. INTRODUCTION

Restoration of defects arising from periodontal disease, infections, trauma, and tumor exeresis remains a major challenge in craniofacial surgery. In such clinical cases, autograft is the "gold-standard" treatment, however the morbidity and the limited availability of bone tissue constrain their use. Allografts have been developed as alternatives to autografts [1]. Collected from human donors, machined allografts are customized to precise dimensions and are available in variable forms, including highly processed decellularized bone derivatives such as mineralized and demineralized bone matrix (DBM), demineralized freeze-dried bone allograft (DFDBA), and freeze-driedbone allograft (FDBA) [2,3].

Decellularised bone derivatives processed from human bone are widely used as bone substitutes. Allogenic bone substitutes obtained after removing the cells, debris, and extracellular matrix proteins retain their porous structure and osteoconductivity, but not osteogenicity and osteoinductivity [4]. Moreover, in bone powder/ particles (BP) formed, these "fully" mineralised substitutes are not easily handled as they are dispersed by irrigation and blood flow during surgery. On the other hand, DBM contains small amounts of calcium-based solids, inorganic phosphates, some traces of cell debris, and proteinaceous components issued from the bone extracellular matrix (i.e., collagen, non-collagenous proteins, and growth factors including BMPs) [5,6], giving it a bone-forming potential. Allogenic DBM exhibits minimal risk of immunogenic reactions [7] and its efficiency is well documented by several preclinical [8-10-9] and clinical studies [11-13]. However, DBM has varying bone-forming efficiencies [14] depending on its harvesting and processing conditions, sterilization methods and storage [15,5,7], carrier use and preparation form [16,14]. DBM is available in powder, particle, sheet, and putty/ paste forms. The latter form is easy to handle and therefore is the

most commonly used. However, conversion of DBM powder to paste by mixing it with a viscous carrier such as hyaluronic acid, carboxymethyl cellulose, poloxamer, calcium sulfate, and so on [17,5,3] has been reported to have several adverse effects, as well as compromising DBM bone-forming efficiency [14]. Therefore, there is an increasing demand for DBM products in paste form, entirely developed from natural bone.

Allogenic bone efficiency also varies depending on the extent of demineralization [18,19].Specifically DBM products to deliver "good" biological performance they have insufficient mechanical stability and, altered ultra-micro-structural properties [19] while the "fully" mineralized bone matrix lacks appropriate osteogenic potential and degradability. Considering these, a partially DBM may be a promising strategy for promoting bone regeneration. Taking these needs into consideration, an allogeneic PDBM has been developed (BioBank®). It is composed of human bone particles which preserve a part of the mineral in the core after demineralization and are included in collagen-rich gelatin, formed by the organic bone phase without added carriers. It is obtained from a cancelous bone of femoral head after decellularision, delipidation, demineralization in HCl and autoclaving at 121°C. It should be noticed that in the paste form, it may be directly injected at the implantation site without prior hydration.

The objective of the present study was to evaluate the osteoformation potential of the new PDBM in rat calvarial defects. It was compared with that of BP before its partial demineralization which was used as a non-demineralized and non-cohesive bone allogenic reference. It is worth noting that rat is a relevant preclinical model to evaluate bone graft substitutes for the repair of craniomaxillofacial defects [20]. Regarding the controversy surrounding the rationale on the use of critical- or subcritical-size defects [21,22], the biological performance of PDBM was evaluated in calvarial size defects. Moreover, the

present study sought to determine whether or not and how the PDBM impacts the early bone healing process in the calvarial defects.

2. MATERIALS AND METHODS

2.1. Partially Demineralized Bone Matrix paste

PDBM and all the other formulations used in the present study were produced and provided by BioBank®. These bone substitutes were derived from discarded femoral heads obtained from healthy living donors, selected according to the clinical and serological criteria. Briefly, collected femoral heads first underwent a supercritical CO_2 patented process (EP3134138B1; BioBank®) that leads to the production of delipidated and viro-inactivated, clinically approved and commercially authorized, bone allografts.

Materials called BP were directly obtained from fractures of cancelous bone issued from the supercrit-treated femoral head after smashing into granules and/or powder particles (0.3 to 1 mm in diameter). BP was used as a non-demineralized and non-cohesive bone allograft reference.

PDBM referred to the material obtained from BP after a specific two-step treatment. This PDBM -the innovative material of interest in this study- was obtained following a process recently patented (EP3134138B1; BIOBank®).

The first step consisted of a partial demineralization of the BP following a liquid HCl treatment (4.5 mmol/g) at room temperature during 90 min. Then, the bone-treated acidic solution was dried under hot air flux in order to generate a partially demineralized bone powder (PDBP). The second step consisted of the hydratation of the PDBP (bone/water, 45/55, w/w) and immediate autoclaving (121°C, 30 min) in certified ISO 13485 conditions

(BIO-STERIL, Saint Germain-Nuelles, 69210 France). The autoclaving step of the PDBM mixed with water ensured both the sterilization and the transformation of the outer demineralized organic phase to gelatin. This high temperature and under-pressure treatment led consequently to a spontaneous organization of the matter to a stable and conformable paste form and assured its sterilization. This new bone material (i.e., PDBM) was then packaged under sterile conditions in a specially designed syringe for direct injection to the implantation site. The main advantages of this formulation process are: i) the preparation method that leads, in one single step, to a sterile material formulated in an interesting paste form, and ii) the clinical potential for the surgeons to use this material directly in clinic without a need for prior (re)hydratation and/or reformulation.

BP, PDBP, and PDBM characteristics were analyzed, compared to each other, and compared to that of totally calcinated BP (BP after heat treatment at 600°C for 8 h) and totally demineralized BP (BP after HCl treatment at 4.5 mmol HCl/g of bone for 3 h), respectively.

Gelatin was provided from Sigma Aldrich (gelatin from porcine skin type A, CAS: 900-70-8).

2.2. Physical and biochemical characterization of the PDBM

2.2.1. Microscopy:

The surfaces of materials were assessed before implantation using digital microscopy (KAYENCE® / VHX-2000F) and environmental scanning electron microscopy (eSEM) (Philips eSEM FEG/XL-30). ESEM examinations were carried out at 15 kV and in a humid atmosphere (approximately from 3 to 5 Torr).

2.2.2. Fourrier transform infrared (FTIR) spectroscopy:

FTIR spectra were obtained using a Brüker-Tensor spectrometer, which is piloted by OPUS software equipped with an MCT (mercury cadmium) detector. The acquisitions were made in

145 absorbance mode on a scale of 500 to 4000 cm^{-1} with a resolution of 2 cm^{-1}. Potassium
146 bromide (KBr) pellets were obtained under vacuum using 1 mg of the samples to test and 200
147 mg of IR grade KBr (0.5%) samples.

148 **2.2.3. Determination of collagen content by hydroxyproline assay:**

149 Collagen content was obtained using a hydroxyproline assay. Lyophilized samples
150 (Msamples) were incubated in 0.1 M acetic acid at 37°C for 48 h, and hydrolyzed by 6 N
151 hydrochloric acid (VWR Chemicals) overnight at 106°C to release hydroxyproline residues.
152 After drying under vacuum, the solid residue was soaked in 1 mL of demineralized water
153 (Vsamples). A different diluted (diluted with a different Factor F) solution of hydroxyproline
154 was oxidized by chloramine T, and was stopped by 3.15 M perchloric acid (Sigma-Aldrich)
155 after 20 min. The addition of dimethylamino-4-benzaldehyde (DMBA) generates a complex
156 which is detected by spectrophotometry. This reaction was carried out at 60°C for 20 min, and
157 was stopped by immersing the tubes in cool water (4°C). The optical density of the aliquots
158 was read using a spectrophotometer at a wavelength of 557 nm and compared with a standard
159 range of trans-4-hydroxy-L-proline (Sigma Aldrich) to determine the concentration of
160 hydroxyproline (Chyp). The following equation determines the collagen concentration of the
161 solutions (Ccoll): Ccoll = Chyp * 7.7*Vsample*F / Msample. Where factor 7.7 represents the
162 converted percentage of hydroxyproline per collagen molecule (13%); F corresponds to
163 dilution factor.

164 **2.2.4. Polarimetry: Optical rotation**:

165 Data were collected using a P-1010 Jasco polarimeter, fitted with a 435 nm filter (this is the
166 usual reference for collagen) and a 1 cm cylinder thermostat (tank-stat). Temperature control
167 was achieved by a Julabo FS18 bath. The optical path was also controlled by Spectra Manager
168 software. Measurements were taken at 27°C. The lyophilized PDBM was solubilized at 20

mg/mL (1.5 mg/mL in collagen according to hydroxyproline assay) with 18 mM acetic acid maintained at 27°C for 2 h before the measurement. The device allows the direct measurement of the angle of optical rotation α_λ expressed in degrees. The amount of helix (X) is derived from the specific optical rotation. And X is derived from [23]:

$$X = [\alpha]_\lambda^{Helix} - [\alpha]_\lambda^{Coil} / ([\alpha]_\lambda^{Collagen} - [\alpha]_\lambda^{Coil})$$

where λ is the wavelength (λ = 435 nm); $[\alpha]_\lambda = \alpha_\lambda / lc$ is the specific optical rotation of the protein in solution; c is the concentration (g/cm^3); l is the optical path (0.1 dm); $[\alpha]_\lambda^{collagen}$ is the specific optical rotation of native soluble collagen (X = 1), which contains only triple helices; and $[\alpha]_\lambda^{Collagen\ coil}$ is the specific optical rotation of the coils (χ = 0) ($[\alpha]_{436nm}^{Collagen}$ = -800 $deg.cm^3.g^{-1}.dm^{-1}$ at 27 °C, $[\alpha]_{436nm}^{Collagen\ coil}$ =-274 deg. $cm^3.g^{-1}.dm^{-1}$ at pH = 7.4 and 40 °C).

2.2.5. Quantification of DNA content:

DNA isolation was done by classical phenol-chloroform from three different types of samples: (i) frozen human femur head (HFH) samples which were crushed, milled, weighed, and lyophilized (n=3), (ii) PDBM which was weighed and lyophilized (n=3), and (iii) bone powder (BP) which was only weighed (n=3). All samples were lysed using proteinase K at 56°C overnight within lysis buffer containing 0.25 M NaCl, 1% SDS, 50 mM Tris, and 5 mM EDTA [24]. The concentration of each extracted DNA sample was determined using the Quant-iT™ PicoGreen dsDNA assay kit (Invitrogen) following the manufacturer's instructions and assessed fluorometrically. Samples of known DNA concentration (in the range 0 to 1 ng /µL) were used to generate the standard curve. When needed, extracted DNA was diluted to ensure that the respective absorbance was within the standard curve range. The DNA quantity was normalized to the initial dry weight of the samples.

2.3.Experimental design and animal model

2.3.1. Animals:

Sixty male, Wistar rats (12 weeks old, 320 to 410 g with mean body weight of 365 g), provided by Janvier Lab, France, were used in this study. The animals were housed at room temperature (20–22°C) and humidity (55%), and were exposed to a 12-hour light/dark cycle (to maintain a normal day/night biological rhythm). They were fed on an *ad libitum* basis with standard laboratory food, and were handled according to the European Guidelines for Care and Use of Laboratory Animals (Directive 2010/63/EU, the European Convention ETS 123, and ARRIVE guidelines). The present animal study was approved by the Ethics Committee 2015072718426555 1'2 (APAFIS#1333).

2.3.2. Experimental design:

To do the radiological and histological evaluations, thirty-six animals randomly distributed (n=6 per group) underwent calvarial defect procedures. In Group I, 8-mm defects on each calvarium were left empty; in Group II, 4- and 6-mm calvarium defects were left empty; in Group III, 8-mm calvarium defects were filled with PDBM paste; in Group IV 8-mm calvarium defects were filled with BP; in Group V, 4- and 6-mm calvarium defects were filled with PDBM bone paste; and in Group VI, 4- and 6-mm calvarium defects were filled with BP. Other thirty-six animals randomly distributed (n=6 per group; a total of 12 per time period, i.e., 3, 7, and 14 days after surgery) were assessed in terms of the expression of target genes.

2.3.3. Animal surgery

2.3.3.1. Anesthesia:

Before the surgery, each rat was first anesthetized by the inhalation of 2% isoflurane and oxygen and then subcutaneously injected with a mixture of Ketamine (IMALGENE®: 40-80 mg/kg weight) and Medetomidine (DOMITOR®: 0.5-1 mg/kg animal weight). As pre-emptive

analgesia, each animal received an intraperitoneal injection of buprenorphine (0.05 mg/kg animal weight).

2.3.3.2. Surgical procedure:

In preparation for surgery, each rat was transferred onto a heating pad, maintained at 37°C on the operating field. Each calvarium was shaved and disinfected using Betadine®. Then, an L-shaped incision was made; the skin and the periosteum consisting two successive layers were elevated and the parietal and frontal calvarium bones were exposed. Afterward, circular bicortical defects were made using trephines (under constant irrigation with physiological saline) and taking care to avoid perforation of the dura mater. The 8-mm-diameter defect was centered on the intersection of the sagittal and coronal sutures. The two 4-mm diameter defects were placed on each parietal bone, whilst the 6-mm defect was located on the frontal bone. Thereafter, each defect site was rinsed with sterile saline and was either left empty or filled with 100 mg of PDBM paste using a specifically designed syringe and applying light pressure or with BP rehydrated with 0.9 NaCl (0.6mL/cc) for 10 min. Finally, the periosteum and skin of the animals were closed with absorbable sutures.

2.3.3.3. Post-surgical animal care:

After surgery, all animals were given the following subcutaneous injections: (i) Buprenorphine, to relieve the pain during the post-operative period; (ii) 5% Baytril®, as prophylactic antibacterial treatment; and (iii) Antisedan® (5 mg/mL), to accelerate awakening. Rats were kept onto the heating pad until awakening. During the postoperative 24 hours, each rat was kept in a separate cage under observation by the animal care personnel. The animals were sacrificed at the determined time points using an overdose of pentobarbital (DOLETHAL®). The calvarial bone was then excised, defleshed, and prepared for analysis.

2.4. In vivo micro-CT analysis

For each animal, a longitudinal analysis of the radiopacity of the calvarial defects, either left empty or filled with PDBM paste, or BP was performed immediately after surgery on days 0, 15, 30, 45, and 60 using a high-resolution, non-invasive, in vivo micro-scanner (micro-CT, Skyscan 1176, Brucker, Aartselaar, Belgium). To do this analysis, the rats were anesthetized using inhaled isoflurane. Images were acquired at the following settings: 50 kV voltage, 476 mA current, exposure time of 40 ms, and a rotation step of 0.7° through a 0.5-mm-thick aluminum filter. The image acquisition time per rat was 6 min. Each three-dimensional (3D) image was reconstructed using a 35-micron average voxel size and using the manufacturer's reconstruction software (NRecon Skyscan 1176, Brucker, Aartselaar, Belgium). 3D visualization was performed with CTVox software (Skyscan 1176, Brucker, Aartselaar, Belgium). Quantitative analysis of the radiopacity volume was also done by DataViewer and CTAn software packages (Skyscan 1176, Brucker, Aartselaar, Belgium). For each rat and each defect of interest in the present study, a cylindrical region of interest (ROI) was fixed at day 0 of the study, corresponding to the diameter of each defect, specifically 4, 6, and 8 mm with a height of 5 mm, and subsequently used as a reference for respective data obtained on days 0, 15, 30, 45, and 60. post-surgery. These ROI dimensions were chosen to take into account all newly formed bone tissues in all cases and time points tested during the healing process. The gray levels corresponding to bone tissue and the PDBM paste and BP were similar; consequently, for the defects that had been left empty, the measured radiopacity presented only the newly formed bone tissue/volume (BV). In the case of defects filled with the PDBM paste, the measured radiopacity presented the sum of both the radiopacity of the biomaterial and that of the newly formed bone tissue.

2.5. Histology and Histomorphometry

The excised calvarial specimens were prepared for non-demineralized histological analysis. Each bone specimen was fixed in 10% neutral-buffered formalin, rinsed with water,

dehydrated using a series of increasing concentrations of ethanol solutions, cleared with xylene, and then embedded in methyl methacrylate. After polymerization, the calvarial bone blocks were oriented to radiography to obtain cross-sections cut parallel to the sagittal plane. Each such section was ground down to a thickness of 300 μm using the exact grinding system (Exakt Apparatebau GmbH Norderstedt, Germany), and polished down to 100 μm. Each section was stained with Stevenel's blue and Van Gienson's picro fuschin before visualization using standard light microscopy.

Images of histological sections were obtained using a light microscope (Olympus Bx 4500) connected to a digital camera (Nikon Coolpix 4500) equipped with a video and image analysis system (NIS Elements BR 2.3, Nikon France S.A.S., France). The images that corresponded to the three successive cross-sections of each defect center were analyzed. To overcome the problem arising from the similarity of bone and material pixels on the digitized and calibrated images, the newly formed bone area and residual particles were delineated manually. The total area of newly formed bone was calculated by adding the areas measured and reported in mm^2.

2.6. Gene expression analyses

Three, 7, and 14 days after surgery, the rats were sacrificed and the calvarial specimens were harvested. The mRNA expression of selected genes was determined quantitatively using RT-PCR as previously described [25]. The tissue inside the 8-mm-diameter defects was retrieved, homogenized, and total RNA was extracted using the TRIzol® Reagent according to the manufacturer's protocol (Invitrogen, France). A NanoDrop spectrophotometer (NanoDrop 1000, Labtech, Palaiseau, France) was used to determine the RNA concentration and purity. After RNA isolation, 500 ng of total RNA was reverse-transcribed into cDNA using the superscript II transcriptase kit (Invitrogen), in which random hexamers were used as primers. Correspondingly, for each time-point of interest, 20 μL of RNA from each sample in the empty calvarium defect group was pooled and reverse transcribed into cDNA to serve as a

reference control. Each RT-PCR analysis was performed in triplicate using 12.5 ng cDNA (RNA equivalent) on the CFX 96 Real-time system (BIORAD Laboratories).

Amplification of the cDNA, using TaqMan® gene expression assays of genes encoding for TNFα (Tumor necrosis factor), IL-1β□□□□□□□□□□□□□□□β □□□E GF (Vascular endothelial growth factor), ANG (Angiogenin), CDH5 (Cadherin 5), PECAM1 (Platelet endothelial cell adhesion molecule), VWF (Von Willebrand factor), ALP (Alkaline phosphatase), RUNX2 (Runt-related transcription factor 2), COLlA1 (alpha-1 type I collagen), BGLAP (Bone gamma-carboxyglutamate protein), SP7 (Sp7 transcription factor), MMP13 (Matrix metalloproteinase 13), OPG (□□ □□ □□□□□□□□□□□□□□□□□□□□□□□□□□□□n cysteine), and TaqMan Universal PCR Master Mix (Applied Biosystems Inc.) was performed by an iCycler thermocycling apparatus (MyiQTM Single-Color Real-Time PCR; Bio-RadLaboratories). All reagents were supplied from Applied Biosystems Inc.: 18s (Hs 99999901_s1), TNFα (Rn 01525859_g1), IL-1β (Rn 00580432_m1), IL-6 (Rn 01410330_m1), IL-8 [cxcl1] (Rn 005578225_m1), VEGF (Rn00582935_m1), ANG (Rn 02349499_g1), CDH5 (Rn 01536708_m1), PECAM1 (Rn 01467262_m1), VWF (Rn 01492158_m1), ALP (Rn 00689814_m1), RUNX2 (Rn 01512298_m1), COL1A1 (Rn 01463848_m1), BGLAP (Rn 01455285_g1), SP7 (Rn 01761789_m1), MMP13 (Rn 01448194_m1), OPG (Rn 00563499_m1), RANKL (Rn 00589289_m1), and SPARC (Rn 00561955_m1). For gene expression measurements, 18s RNA endogenous control (house-keeping gene with a constant expression level) was used as an internal control. Additionally, relative gene expression was calculated using the ΔΔCt

315 method by normalizing the Ct value of each gene at each time-point to the Ct value of the
316 corresponding pooled sample.

317 **2.7. Statistical analyses**

318 Numerical values of the volume of regenerated bone within the defects, as well as the RT-PCR
319 results of interest in the present study are reported as mean value ± standard deviation (SD).
320 Statistical analysis was performed using the Student's unpaired t-test. Furthermore, differences
321 with *P*-value < 0.05 were considered statistically significant.

322 **3. RESULTS**

323 **3.1. PDBM characterization**

324 In digital microscopy, the partially demineralized bone matrix (PDBM) paste and the bone
325 powder (BP) showed different forms (Figure 1A and 1D). In escanning electron microscope
326 (eSEM), the PDBM showed an amorphous structure devoid of collagen fibers (Figure 1B-C)
327 while BP exhibited small particles consisting collagen bundles with different orientations
328 (Figure 1E and 1F). The efficiency of the decellularization was evaluated by the quantification
329 of residual DNA in human femoral heads (HFH), BP, and PDBM. DNA level was
330 significantly ($p< 0.05$) reduced in PDBM (2.22 ± 0.33 ng /mg) and in BP (0.55 ± 0.03 ng/mg)
331 compared to the pertinent results obtained from HFH (296.9 ± 74.33 ng/mg) (Figure 1G). The
332 DNA level was considerably ($p< 0.05$) lower than the 50 ng/mg threshold [26] in both PDBM
333 and BP.

334 PDBM paste was further analyzed with Fourier transform infrared (FTIR) and compared with
335 that of the BP, fully calcinated or totally demineralized. The absorption bands located at 1655
336 and 1565 cm^{-1} corresponded to the amide I and amide II, respectively. The peak around 1450
337 cm^{-1} was attributed to the carbonate. While the peak at 1000 and the double peaks at 657 and
338 577 cm^{-1} were attributed to the phosphate contents v_1 and v_4, respectively (Figure 1H). As
339 expected, in the calcinated BP, amide I and amide II bands were totally eliminated. In the

completely demineralized form of the BP, the two organic bands were the unique compounds preserved. In contrast with both bands in the BP, as in the PDBM paste, the two organic and the four inorganic components were present. However, it is worth to note that in the PDBM paste, the bands present in the spectrum were similar though the intensity was different. The proportion of amide peaks to inorganic compounds was more attenuated in the PDBM paste compared to the BP. This result confirms the loss of part of the inorganic phase and subsequently the increase of the relative contribution of the organic phase in the PDBM paste in comparison with the BP.

The organic phase of PDBM was analyzed by hydroxyproline content, and collagen type I was further characterized by optical ellipsometry. The quantity of "collagenic phase" extractible from the BP and the PDBP (the partially demineralized form of BP) was 0.005 mg/mg product and 0.009 mg/mg product, respectively. In the PDBM paste, the relative quantity of accessible collagenic phase was still weak (0.073 mg/mg product) though significantly higher (Figure 1I). It was compatible to compare these experimentally observed values with the collagen amount expected from theoretical calculations; 0.3 mg/mg, 0.23 mg/mg, and 0.46 mg/mg for BP, PDBP, and the PDBM paste, respectively. Interestingly, the percentage of accessible collagenic fraction on BP and PDBP was less than 2% (0.005/0.3 = 1.66%; 0.009/0.46 = 1.96% for BP and PDBP, respectively), whereas this amount reached more than 30% in the PDBM paste (0.073/0.23 = 31.7%). This result demonstrated that the organic phase accessible from the PDBM matrix was 15 times higher than that in the powder form of the material. In conclusion, the biochemical analysis suggested that the thermic process increased the "accessibility" of the organic phase. The organic phase extracted from PDBM was characterized in polarimetry via measuring the optical rotation. The values of the optical rotation measured by polarimetry at 435 nm compared to native collagen in the same conditions allowed to estimate the amount of helix alpha in the biochemical structure of

PDBM paste (Table 1). The quantity found (only 13%) suggested that the organic phase of PDBM was mainly constituted by collagen fragments like gelatin. Moreover, ellipsometry measurements in various temperature conditions showed that the rotary power of PDBM (reflecting the presence of helix alpha within collagen) was similar to that observed in gelatin, suggesting that the organic phase of PDBM was mainly constituted by collagen fragments.

3.2. Clinical observation

All animals regained their ambulatory capabilities within 2-3 hours after surgery. All surgical wounds healed uneventfully. Moreover, there were no changes in the animal body weight, behavior, and in the overall animal health during the 8-weeks post-surgery period.

3.3. Bone repair kinetics

To study the bone healing as a function of the size of calvarial defect, critical 8-mm-diameter and subcritical, specifically, 6-, 4-mm-diameter defects on the same rat in a multi-defect calvarial model was used. *In vivo* micro-CT scans of the defects either filled or not filled with BP or PDBM paste was immediately made after surgery at day 0 (D0) and during the 2^{nd}, 4^{th}, 6^{th}, and 8^{th} weeks post-surgery. In the empty 8-mm-diameter defects, only small areas of radiopacity were observed mainly along the borders during the entire healing period (Figure 2A1). In the BP-filled defects, radiopacity area decreased from D0 to D15 (Figure 2A2). while in the PDBM-filled defects, radiopacity areas were present as early as the 2^{nd} week after surgery (Figure 2A3). In the PDBM-filled defects, compared to D0, the radiopacity volume (evidence for the residual implanted material and the new formed bone volume) was significantly ($p<0.05$) increased by 2 folds at the 2^{nd} week and reached a plateau at the 4^{th} week post-surgery (Figure 2B). Compared to the empty defects and the BP-filled defects, the radiopacity in the PDBM paste-filled defects was significantly ($p<0.05$) increased, for exemple by 3.5 folds (16.64 ± 6.9 mm^3 and 22.2 ± 6.4 mm^3 *vs.* 4.87 ± 3.72 mm^3, and 6.27 ± 5.09 mm^3 for the PDBM paste-filled and empty defects, respectively, at the 4^{th} and 8^{th} weeks

post-surgery) (Figure 2B). These results provided evidence that PDBM notably promoted new bone formation.

The radiopacity areas increased along with the healing time in 6-mm-diameter defects left empty and in PDBM paste-filled defects; while in the BP-filled defects, the radiopacity decreased from D0 to D15 (Figure 3A). New bone formation, especially in the frontal area of the empty defects, was present at the 2nd post-surgery week, which improved thereafter and attained a plateau at the 4th week (Figure 3A1). The animal group which had received the PDBM paste exhibited significant improvement ($p<0.05$) in every defect at all time-points tested (6.23 mm^3 ± 1.17 vs 22.15 mm^3 ± 3.45 at D0 and D60, respectively; Figure 3B). At D60, compared to the empty- and BP-filled defects, the defects filled with PDBM paste exhibited a significant increase ($p<0.05$) in radiopacity volume (almost 3-folds; Figure 3B). In vivo micro-CT scans, monitoring the subcritical-size defects, revealed that the 6-mm- and 4-mm-diameter empty calvarial defects exhibited a different time course of the bone healing process (Figure 3A). In the case of 4-mm diameter defects, the radiopacity volume also increased over the time course of healing process in both animal groups tested (Figure 3A). Two 4-mm-diameter calvarial defects were created bilaterally in both animal groups tested (specifically the controls and those filled with BP or PDBM paste). Comparison of the results from the two empty defects located in the same rat revealed differences related to the incision location and the flap: in defects away from the flap incision, increased bone formation was systematically observed over the time period of the present study in all defects in contrast to the defects close to the lateral flap incision (Figure 3A). The radiopacity volume increased in the empty defects of the rats in the control group over time and was similar to that observed for the defects filled with BP or PDBM paste in the treated rat group (Figure 3C).

3.4. New bone formation

After 8 weeks of implantation, in the empty and BP-filled 8-mm-diameter defects, newly formed bone was observed mainly at the edge of the defects (Figure 4A and 4B). On the contrary, new bone formation in the defects filled with the PDBM paste was localized both at the edges and in the center of the defects around remnants of PDBM paste (identified as varying-size particles of bone with cell-free lacunas) (Figure 4C and 4D). Quantitative analysis confirmed radiological findings in that a considerable amount of bone was formed. In other words, bone area was significantly increased ($p<0.05$) specifically by 16.34 times and 2.16 times, compared to that observed in the defects that had remained empty or filled with BP (specifically, 1.02 ± 0.32 mm^2 vs 0.06 ± 0.05 mm^2 and 0.47 ± 0.5 mm^2 respectively) (Figure 4E). In the case of the 6mm-diameter-PDBM-filled defects, a newlyformed bone was observed throughout the filled defects. The newly formed bone was either surrounding or bridging the particles from the edge to the central area of the defect, while it was mainly located at the periphery of the empty and the BP-filled defects (Figure 5A, 5B and 5C). Lacuna containing osteocytelike and some lining cells, as well as blood vessels and bone marrow were observed in the newly formed bone (Figure 5D). The area of the newly formed bone was significantly ($p<0.05$) greater (by about 1.6 times and 2.58 times) in the defects filled with the PDBM paste than those in the defects left empty or filled with BP (specifically, 1.96 ± 0.81 mm^2 vs 1.24 ± 0.75 mm^2 and 0.76 ± 0.52 mm^2 respectively) (Figure 5E). In the case of the 4-mm-diameter defects, the new bone formed in the empty defects (located away from the flap incision) had almost filled entirely these defects (Figure 6A, 6B and. 6C). Quantitative analysis showed that the amount of newly formed bone was similar in the empty, BP and PDBM-paste-filled defects (Figure 6D). None of the defects exhibited inflammation or foreign body reaction.

3.5. Expression of selected inflammation-, angiogenesis- and bone-related genes

To determine whether and how PDBM affects the early stages of intramembranous bone regeneration, the expression of selected genes in 8-mm-diameter-PDBM-filled defects was

compared to those expressed in empty same-diameter ones at 3, 7, and 14 days after implantation.

Gene expression of inflammatory markers: The time course of TNFα, IL-1β, IL-6, and IL-8 mRNA expression in both empty- and PDBM-filled defects increased from D3 to D7 exhibited a peak at D7 and decreased thereafter (for up to 14 days) (Figure 7A, B). Compared to the respective results obtained from the empty defects, the PDBM-filled ones exhibited significant upregulated expression (by 2.5 and 6.8 folds; p=0.003 and p=0.01, respectively) of the TNFα gene at D3 and D7 (Figure 7A). IL-6 and IL-8 genes were also upregulated (by 4.7 and 4 folds; p= 0.046 and 0.036, respectively) only at D3 post-surgery (Figure 7B). On the contrary, IL-6 expression was significantly down-regulated at D7 (p= 0.02; Figure 7B). Non-significant difference was observed in the expression level of IL-1β gene in both groups tested; that is, the expression was similar at all time-points checked (Figure 7A).

Gene expression of angiogenesis markers: Expression of angiogenesis markers showed a similar temporal trend to that of inflammatory markers in both empty and PDBM-filled defects (Figure 7C, D). Expression of VEGF, ANG, CDH5, PECAM1, and VWF genes exhibited a peak level at D7 post-surgery. Moreover, the expression of all aforementioned genes was increased from D3 to D7 and decreased thereafter. Compared to the empty defects, the expression levels of VEGF and VWF in the PDBM-filled defects were significantly increased at D3 (p=0.019 and p=0.014, respectively; Figure 7D). Expression of the ANG gene increased at D7 (p=0.036), while that of CDH5 was downregulated at D14 (p= 0.007; Figure7C). Moreover, the expression levels of all angiogenesis markers selected for the empty and PDBM-filled defects were similar for all other time-points tested.

Expression of genes pertinent to bone formation and remodeling: RUNX2, MMP13, RANKL, and SPARC genes were upregulated in the empty defects, from D3 to D7 post-surgery (Figure 8B, C). The presence of PDBM affected these outcomes. Compared to the

464 results obtained from the empty defects, expression of the ALP, BGLAP, SP7, and RUNX2
465 genes in the PDBM-filled defects was significantly higher at D3 (p= 0.004, 0.02, 0.015, and
466 0.008, respectively; Figure 8A and B). From D3 to D7, only the expression of ALP, BGLAP,
467 SP7, RUNX2, COL1A1, and RANKL genes was decreased (Figure 8A, B, and C); while the
468 expression of other genes tested was similar during those days. From D7 to D14, only the
469 expression of RANKL gene was significantly increased (p= 0.001; Figure 8C). The presence
470 of PDBM in the defects differently affected the expression of aforementioned genes over time.
471 Specifically, the expression of the genes ALP (D3), RUNX2 (D3), BGLAP (D3), SP7 (D3),
472 and RANKL (D14) was significantly up-regulated (p= 0.004, 0.02, 0.015, and 0.016,
473 respectively) by the presence of PDBM in the calvarium defects tested. In contrast, the
474 expression of ALP (D7 and D14), BGLAP (D14), SP7 (D14), COL1A1(D7), OPG (D7), and
475 SPARC (D7) was significantly down-regulated (p= 0.04, 0.03, 0.012, 0.016, 0.013, 0.011 and
476 0.001, respectively; Figure 8A, B, and C).

477 **4. DISCUSSION**

478 Allogenic demineralized bone matrix (DBM) is regarded as a viable alternative option for
479 autografts ([5,3]. Its use is increasing and different formulations are constantly
480 emerging;however, at the present time, conditions under which DBM exhibits optimal
481 osteoforming activity remain elusive. The present study investigated for the first to our
482 knowledge the *in vivo* response of a new formulation of allogenic partially DBM (PDBM). It
483 was prepared from cancelous bone of femoral heads after decellularision, delipidation, and
484 demineralizion in HCl, as well as autoclaving at 121°C. It consisted of partially demineralized
485 bone particles (PDBP), in a collagen-rich gelatin, formed by the organic bone phase without
486 added carriers. The biological performance of PDBM paste was studied in healing the bone
487 defect in the rat calvarium model, in critical- and subcritical-size calvarial defects, in
488 comparison to that of the BP before its partial demineralization, which was used as a non-

489 demineralized and non-cohesive bone allograft reference. Results obtained showed that the
490 new PDBM paste had an enchanced clinical use (ready-to-use, easy-to-handle, moldable, and
491 cohesive), influenced the early critical events involved in bone regeneration, and exhibited
492 efficient bone forming capacity in critical-size calvarial defects.
493
494 In contrast to BP, PDBM paste promoted bone healing in 6- and 8- mm-diameter calvarial
495 bone defects, both considered critical-sized [21,22]. As expected, the extent of new bone
496 formation was decreased by increasing the size of the defect. However, PDBM paste presence
497 showed to be crucial for the repair of the 8-mm defects, as the amount of newly formed bone
498 in defects filled with PDBM was increased by about 16.5 folds compared to that of defects left
499 empty at 8 weeks post-implantation. Bone healing was accelerated in 6-mm defects left empty,
500 and after PDBM addition the new bone formation augmented only 1.6 folds. While, in the 4-
501 mm defects, the closure was observed regardless of the PDBM presence, showing that the use
502 of PDBM was not clinically effective in regenerating small defects. It is interesting to note that
503 no new bone formation in contact to or around the BP was observed regardeless of the size of
504 the bone defect. Moreover, in the critical-size PDBM-filled defects, the bone formation was
505 enhanced as the radiopacity volume was significantly increased ($p<0.05$) already at the 2nd
506 week post-surgery, suggesting that PDBM may be also clinically effective in shortening the
507 time required for bone healing after surgery. Some studies have investigated the potential of
508 allogenic DBM in the same animal model and reported contradictory results. For instance, in
509 the 8-mm-diameter defects, DBM showed significant bone-forming capacity [18,8,10] while
510 others showed limited capability [27-29]. Direct comparison between the results of this study
511 and the aforementioned published reports is thus not possible due to differences in the DBM
512 formulations, as well as the outcome measures.

513 The bone-forming potential of PDBM paste may be attributed to several factors including
514 enhanced clinical use. It displays improved surgical handling properties, adaptation to the
515 uneven walls of the bone defects and cohesive between the particles properties without
516 drawbacks of added carriers. Paste form was obtained entirely from bone and showed a
517 significant bone-forming advantage over human BP. Carriers (e.g., hyaluronic acid,
518 carboxymethylcellulose, glycerol, calcium sulfate, gelatin, etc.) used to turn DBM powder to
519 paste or putty forms [30,3] have been reported to compromise DBM clinical performance by
520 decreasing the amount of the active DBM components [16,14] and/or by adverse effects such
521 as inflammation [31,32].

522 In histology, the PDBM paste showed typical osteoconductive phenomena, including newly-
523 formed bone at the defect edges and around the PDBM remnants (Figure 5C), probably due to
524 both the partially demineralized bone particles and the collagen-rich gelatin.. DBM
525 osteoconductivity has been reported as the primary mechanism for supporting the DBM-
526 associated bone formation [5,10], and gelatin derived from the collagen hydrolysis has been
527 shown to be highly biocompatible and biodegradable [33] and plays a role in promoting cell
528 adhesion. Moreover, PDBM has been displayed better applicability than un-demineralized or
529 full DBM [19], and in contrast to full DBM, PDBM particles could act in a more bone-like
530 manner, providing immediate structural support to unstable osseous defects.

531 Bone forming capacity of DBM is also attributed to its osteoinductivity [5,34]. In the present
532 study, the bone formation in the center of the PDBM-filled critical-sized defects could suggest
533 a slight osteoinductive potential though further confirmatory evaluation with heterotopic
534 implantation is required. Moreover, in the PDBM-filled defects, the expression of RUNX2,
535 ALP, SP7, and BGLAP genes was upregulated 3 days after surgery. These genes are closely
536 related to osteogenesis [35,36] and their upregulated expression under the effect of PDBM in
537 the bone defect could signify the recruitment and/or enhanced differentiation of

538 osteoprogenitor cells. However, osteoinduction implication in the cellular behavior is unlikely
539 as PDBM paste was obtained with autoclaving the PDBP, a process that denaturates growth
540 factors, including BMPs, which are released during demineralization and therefore abolishes
541 their "osteoinduction" properties.

542 Indeed, autoclaving is a key and puzzling point for the mechanisms underlying the
543 osteoformation capacity of the PDBM paste observed in the present study. Autoclaved
544 autografts or allografts have been used to reconstruct bone with interesting results [37,38]
545 while it has been reported that in addition to the denaturation of bone organic matrix,
546 autoclaving also alters its mechanical and structural properties [39,40]. Consequently, in the
547 present study autoclaving the PDBP, in addition to transforming the outer demineralized
548 organic phase in a collagen-rich gelatin probably modifies the structural and biomechanical
549 properties of the mineral part preserved in the core, thereby influencing the cell behavior in a
550 multifacet manner. For instance, it has been reported that pepsin-digested and solubilized
551 DBM hydrogel allows osteoprogenitors proliferation [41] and denaturated collagen promotes
552 fibroblast survival [42] while partially demineralized displays better osteoprogenitor adhesion
553 and proliferation than those completely demineralized [19]. It is logical therefore to consider
554 that in the osteoformation capacity of the PDBM is involved an overall effect of the material,
555 paste structure, mechanical properties, and constitutive molecules. Further comparison of the
556 potential of PDBM paste with those of the PDBP before autoclaving and fully DBP *in vivo*
557 and the comparison of the osteoprogenitor behavior towards such subsitutes is necessary to
558 decipher umechanisms involved in the osteoconduction/ osteoinduction process.

559 Besides the osteogenesis -related genes, another main finding of the present study that pointed
560 out the PDBM influence in the early critical events involved in bone regeneration was that
561 PDBM differently modulated the expression of genes pertinent to inflammation and
562 angiogenesis at days 3 and 7 post-surgery. Proinflammatory cytokines such as TNFα, IL-1, IL-

6, and IL-8, which mainly contribute to the initiation of the healing process by recruiting macrophages and osteoprogenitor cells from their local niches [43-45], were highly expressed in empty-left defects, reflecting inflammation during the early wound healing [46]. In the PDBM-filled defects, the overall increase of the aforementioned gene expression levels clearly indicated that the PDBM promoted immuno-inflammatory mechanisms at least at gene level and might be involved in the early recruitment of mesenchymal stem cells and osteoprogenitor cells. Moreover, we observed that the angiogenesis-related genes exhibited a temporal trend similar to that of inflammation, that is, a trend towards higher expression at D7 and a reduction at D14, which corresponds with the gradual process of maturation from the granulation tissue to woven bone formation taking place between days 7 and 14 [46]. PDBM significantly upregulated the expression level of VEGF and VWF at D3 and that of ANG at D7. Above all, VEGF is a signaling protein that is induced during the inflammation phase within the surrounding bone cells or recruited inflammatory cells [47,48], initiates macrophage-related angiogenic responses [49], and is a crucial factor in angiogenesis-osteogenesis coupling during intramembranous ossification-mediated bone healing [50].

The present study showed for the first time the PDBM–associated modifications of the transcriptional profile pertinent to bone repair ; however, it suffers some limitations. Firstly, the gene expression profile has to be associated with histology and immunohistochemistry to further understand the PDBM impact on the early healing. Secondly, the harvested tissue comprised various cell types, making difficult to localize the source of the gene expression within the defects. Lastly, the identification of genes in later time points should also be analyzed.

5. CONCLUSION

Results of the present study indicated the characterization and the biological performance of a new PDBM paste. PDBM consists of PDBP in a collagen-rich gelatin, formed by the organic

588 bone phase without added carriers. This formulation included the preparation of the cancelous
589 bone from femoral head after decellularision, delipidation, and demineralization in HCl, as
590 well as autoclaving at 121°C, a process that ensures both the sterilization and transformation
591 of the outer organic phase of the PDBP to gelatin. It exhibits many advantages for the
592 clinicians, that is providing a ready-to-use, easy-to-handle, moldable, and cohesive paste,
593 which can be packed into bone defects and resists against irrigation and bleeding during
594 surgery. Implanted in critical-size calvarial defects, it also exhibits a bone-forming capacity in
595 contrast to BP which before demineralization failed to show any new bone formation capacity
596 in both critical- and subcritical-size calvarial defects. The comparison of the transcriptional
597 profile of genes in 8-mm-diameter-PDBM-filled defects to that of genes in empty defects
598 showed that PDBM deeply influences the early critical events involved in bone regeneration.
599 The PDBM efficient bone formation capacity makes it an attractive graft option for treating
600 the defects in periodontal and maxillofacial areas.

601

602

603 **Acknowledgments**

604 We gratefully acknowledge the help of Prof. Rena Bizios for critically review of the paper. We
605 also thank Nathanael Larochette and Hanane El-Hafci for their technical support.

606 **Formatting of funding sources**

607 This study was supported by Campus France, and "Fondation des Gueules Cassées" [N° 53,
608 2018].

609 **Author contributions:** AMD : design, data research, analysis, and interpretation and
610 manuscript writing; MB and HP : data research, analysis and interpretation and critically read
611 the manuscript; SR, BM and EP: data research, analysis, and interpretation regarding material

612 characterization; RB: provided bone substitutes used; HMB: critically read the manuscript;
613 FA: conception, design, data analysis and interpretation and manuscript writing/ editing.

614 **Conflict of interest:**

615 AMD, HP, HMB, FA declare that they have no conflicts of interest

616 SR work at c and d

617

618

619

620 **REFERENCES**

621 [1] V. Campana, G. Milano, E. Pagano, M. Barba, C. Cicione, G. Salonna, W. Lattanzi, G.
622 Logroscino, Bone substitutes in orthopaedic surgery: from basic science to clinical
623 practice, Journal of Materials Science: Materials in Medicine 25 (2014) 2445-61. doi:
624 10.1007/s10856-014-5240-2.

625 [2] W. Wang, K.W.K. Yeung, Bone grafts and biomaterials substitutes for bone defect
626 repair: A review, Bioactive Materials 2 (2017) 224-247. doi:
627 10.1016/j.bioactmat.2017.05.007.

628 [3] H. Zhang, L. Yang, X.G. Yang, F. Wang, J.T. Feng, K.C. Hua, Q. Li, Y.C. Hu,
629 Demineralized Bone Matrix Carriers and their Clinical Applications: An Overview,
630 Orthopaedic Surgery 11 (2019) 725-737. doi: 10.1111/os.12509.

631 [4] P. Baldwin, L.J Deborah, D.A Auston, M.S. Hassan, R.S. Yoon, K.J. Kenneth.
632 Autograft, Allograft, and Bone Graft Substitutes: Clinical Evidence and Indications for
633 Use in the Setting of Orthopaedic Trauma Surgery, Journal of Orthopaedic Trauma 4
634 (2019) 203-213. doi: 10.1097/BOT.0000000000001420.

635 [5] E. Gruskin, B.A. Doll, F.W. Futrell, J.P. Schmitz, J.O. Hollinger, Demineralized bone
636 matrix in bone repair: history and use, Advanced Drug Delivery Reviews 64 (2012)
637 1063-77. doi: 10.1016/j.addr.2012.06.008.

638 [6] M.G. Gonzaga, B.G. Dos Santos Kotake, F.A.T. de Figueiredo, S. Feldman, E.
639 Ervolino, M.C.G. Dos Santos, J.P.M. Issa, Effectiveness of rhBMP-2 association to
640 autogenous, allogeneic, and heterologous bone grafts, Microscopy Research and
641 Technique 82 (2019) 689-695. doi: 10.1002/jemt.23215.

642 [7] N. Bhamb, L.E.A. Kanim, S. Drapeau, S. Mohan, E. Vasquez, D. Shimko, W.
643 McKAY, H.W. Bae, Comparative Efficacy of Commonly Available Human Bone
644 Graft Substitutes as Tested for Posterolateral Fusion in an Athymic Rat Model,
645 International Journal of Spine Surgery 13 (2019) 437-458. doi: 10.14444/6059.

646 [8] N. Mokbel, C. Bou Serhal, G. Matni, N. Naaman, Healing patterns of critical size bony
647 defects in rat following bone graft, Journal of Oral and Maxillofacial Surgery, 12
648 (2008) 73-8. doi: 10.1007/s10006-008-0107-7.

649 [9] C.I.A. Van Houdt, DA. Cardoso, B.A.J.A. van Oirschot, D.J.O. Ulrich, J.A. Jansen,
650 S.C.G. Leeuwenburgh, J.J.J.P. van den Beucken, Porous titanium scaffolds with
651 injectable hyaluronic acid-DBM gel for bone substitution in a rat critical-sized
652 calvarial defect model, Journal of Tissue Engineering and Regenerative Medicine 11
653 (2017) 2537-2548. doi: 10.1002/term.2151.

654 [10] A. Sindel, Ö. Dereci, H.S. Toru, S. Tozoğlu, Histomorphometric Comparison of Bone
655 Regeneration in Critical-Sized Bone Defects Using Demineralized Bone Matrix,
656 Platelet-Rich Fibrin, and Hyaluronic Acid as Bone Substitutes, The Journal of
657 craniofacial surgery 28 (2017) 1865-1868. doi: 10.1097/SCS.0000000000003588.

658 [11] C.A. Serrano Méndez, N.P. Lang, M. Caneva, G. Ramírez Lemus, G. Mora Solano, D.
659 Botticelli, Comparison of allografts and xenografts used for alveolar ridge

660 preservation. A clinical and histomorphometric RCT in humans, Clinical Implant
661 Dentistry and Related Research 19 (2017) 608-615. doi: 10.1111/cid.12490.
662 [12] Ö. Solakoglu, W. Götz, G. Heydecke, H. Schwarzenbach, Histological and
663 immunohistochemical comparison of two different allogeneic bone grafting materials
664 for alveolar ridge reconstruction: A prospective randomized trial in humans, Clinical
665 Implant Dentistry and Related Research 21 (2019) 1002-1016. doi: 10.1111/cid.12824.
666 [13] A. Patel, H. Greenwell, M. Hill, B. Shumway, A. Radmall, Ridge Augmentation
667 Comparing an Allograft Plus Autogenous Bone Chips to an Osteoinductive
668 Demineralized Bone Matrix: A Clinical and Histologic Study in Humans, Implant
669 Dentistry 28 (2019) 613-620. doi: 10.1097/ID.0000000000000925.
670 [14] N. Russell, W.R. Walsh, V. Lovric, P. Kim, J.H. Chen, M.J. Larson, F. Vizesi, In-vivo
671 Performance of Seven Commercially Available Demineralized Bone Matrix Fiber and
672 Putty Products in a Rat Posterolateral Fusion Model, Frontiers in Surgery (2020) 7:10.
673 doi: 10.3389/fsurg.2020.00010.
674 [15] S.D. Ferreira, W.S. Dernell, B.E. Powers, R.A. Schochet, C.A. Kuntz, S.J. Withrow,
675 R.M. Wilkins, Effect of gas-plasma sterilization on the osteoinductive capacity of
676 demineralized bone matrix, Clinical Orthopaedics and Related Research 388 (2001)
677 233-9. doi: 10.1097/00003086-200107000-00032.
678 [16] K.J. Lee, J.G. Roper, J.C. Wang, Demineralized bone matrix and spinal arthrodesis,
679 The Spine Journal: official journal of the North American Spine Society 5 (2005)
680 217S-223S. doi: 10.1016/j.spinee.2005.02.006.
681 [17] S.T. Moore, J.M. Katz, R.M. Zhukauskas, R.M. Hernandez, C.S. Lewis, P.R.
682 Supronowicz, E. Gill, S.M. Grover, N.S. Long, R.R. Cobb, Osteoconductivity and
683 osteoinductivity of Puros (R) DBM putty, Journal of Biomaterials Applications 26
684 (2011) 151-71. doi: 10.1177/0885328210366061.

685 [18] J.W. Turonis, J.C. 3rd. McPherson, M.F. Cuenin, S.D. Hokett, M.E. Peacock, M.
686 Sharawy, The effect of residual calcium in decalcified freeze-dried bone allograft in a
687 critical-sized defect in the Rattus norvegicus calvarium, The Journal of oral
688 implantology 32 (2006) 55-62. doi: 10.1563/780.1.
689 [19] S. Liu, Y. Wang, J. Wang, P. Qiu, S. Wang, Y. Shi, M. Li, P. Chen, X. Lin, X. Fang, A
690 cancellous bone matrix system with specific mineralisation degrees for mesenchymal
691 stem cell differentiation and bone regeneration, Biomaterials Science 6 (2019) 2452-
692 2467. doi: 10.1039/c8bm01657g.
693 [20] P.P. Spicer, J.D. Kretlow, S. Young, J.A. Jansen, F.K. Kasper, A.G. Mikos, Evaluation
694 of bone regeneration using the rat critical size calvarial defect, Nature Protocols 7
695 (2012) 1918-29. doi: 10.1038/nprot.2012.113.
696 [21] A. Vajgel, N. Mardas, B.C. Farias, A. Petrie, R. Cimões, N. Donos, A systematic
697 review on the critical size defect model, Clinical Oral Implants Research 25 (2014)
698 879-93. doi: 10.1111/clr.12194.
699 [22] P.S. Gomes, M.H. Fernandes, Rodent models in bone-related research: the relevance of
700 calvarial defects in the assessment of bone regeneration strategies, Laboratory Animals
701 45 (2011) 14-24. doi: 10.1258/la.2010.010085.
702 [23] S. Giraudier, D. Hellio, M. Djabourov, V. Larreta-Garde, Influence of weak and
703 covalent bonds on formation and hydrolysis of gelatin networks, Biomacromolecules,
704 5 (2004) 1662-6. doi: 10.1021/bm049670d.
705 [24] M. Bensidhoum, A. Chapel, S. Francois, C. Demarquay, C. Mazurier, L. Fouillard, S.
706 Bouchet, J.M. Bertho, P. Gourmelon, J. Aigueperse, P. Charbord, N.C. Gorin, D.
707 Thierry, M. Lopez, Homing of in vitro expanded Stro-1- or Stro-1+ human
708 mesenchymal stem cells into the NOD/SCID mouse and their role in supporting human
709 CD34 cell engraftment, Blood 103 (2004) 3313-9. doi: 10.1182/blood-2003-04-1121.

[25] K. Vandamme, X. Holy, M. Bensidhoum, M. Deschepper, D. Logeart-Avramoglou, I. Naert, J. Duyck, H. Petite, Impaired osteoblastogenesis potential of progenitor cells in skeletal unloading is associated with alterations in angiogenic and energy metabolism profile, Bio-medical Materials and Engineering 22 (2012) 219-26. doi: 10.3233/BME-2012-0711.

[26] P.M. Crapo, T.W. Gilbert, SF. Badylak, An overview of tissue and whole organ decellularization processes, Biomaterials 32 (2011) 3233-43. doi: 10.1016/j.biomaterials.2011.01.057.

[27] B.W. Stancoven, J. Lee, D.R. Dixon, J.C. 3rd. McPherson, F.C. Bisch, U.M. Wikesjö, C. Susin, Effect of bone morphogenetic protein-2, demineralized bone matrix and systemic parathyroid hormone (1-34) on local bone formation in a rat calvaria critical-size defect model, Journal of Periodontal Research 48 (2013) 243-51. doi: 10.1111/jre.12001.

[28] H.P. Kim, Y.H. Ji, S.C. Rhee, E.S. Dhong, S.H. Park, E.S. Yoon, Enhancement of bone regeneration using osteogenic-induced adipose-derived stem cells combined with demineralized bone matrix in a rat critically-sized calvarial defect model, Current Stem Cell Research & Therapy 7 (2012) 165-72. doi: 10.2174/157488812799859847.

[29] G. Intini, S. Andreana, R.J. Buhite, L.A. Bobek, A comparative analysis of bone formation induced by human demineralized freeze-dried bone and enamel matrix derivative in rat calvaria critical-size bone defects, Journal of Periodontology 79 (2008) 1217-24. doi: 10.1902/jop.2008.070435.

[30] J.A. Shehadi, S.M. Elzein, Review of commercially available demineralized bone matrix products for spinal fusions: A selection paradigm, Surgical Neurology International 8 (2017) 203. doi: 10.4103/sni.sni_155_17.

[31] M.P. Bostrom, X. Yang, M. Kennan, H. Sandhu, E. Dicarlo, J.M. Lane, An unexpected outcome during testing of commercially available demineralized bone graft materials: how safe are the nonallograft components? Spine (Phila Pa 1976) 26 (2001) 1425-8. doi: 10.1097/00007632-200107010-00007.

[32] D.C. Markel, S.T. Guthrie, B. Wu, Z. Song, P.H. Wooley, Characterization of the inflammatory response to four commercial bone graft substitutes using a murine biocompatibility model, Journal of Inflammation Research 5 (2012) 13-8. doi: 10.2147/JIR.S21411.

[33] M. Santoro, A.M. Tatara, A.G. Mikos, Gelatin carriers for drug and cell delivery in tissue engineering, Journal of Controlled Release 190 (2014) 210-8. doi: 10.1016/j.jconrel.2014.04.014.

[34] T. Al Kayal, D. Panetta, B. Canciani, P. Losi, M. Tripodi, S. Burchielli, P. Ottoni, P.A. Salvadori, G. Soldani, Evaluation of the effect of a gamma irradiated DBM-pluronic F127 composite on bone regeneration in Wistar rat, PLOS One 10 (2015) e0125110. doi: 10.1371/journal.pone.0125110.

[35] L. Wang, Z.Y. Li, Y.P. Wang, Z.H. Wu, B. Yu, Dynamic Expression Profiles of Marker Genes in Osteogenic Differentiation of Human Bone Marrow-derived Mesenchymal Stem Cells, Chinese Medical Sciences Journal 30 (2015) 108-13. doi: 10.1016/s1001-9294(15)30021-3.

[36] J. Freitas, S.G. Santos, R.M. Gonçalves, J.H. Teixeira, M.A. Barbosa, M.I. Almeida, Genetically Engineered-MSC Therapies for Non-unions, Delayed Unions and Critical-size Bone Defects, International Journal of Molecular Sciences 20 (2019) 3430. doi: 10.3390/ijms20143430.

[37] T. Inokuchi, H. Ninomiya, R. Hironaka, S. Yoshida, M. Araki, K. Sano, Studies on heat treatment for immediate reimplantation of resected bone, Journal of Cranio-Maxillo-Facial Surgery 19 (1991) 31–39. doi: 10.1016/s1010-5182(05)80269-0.

[38] S. Menon, K. Banu, R. Veena, V. Srihari, M.E. Sham, M. Vinay, The Recycling of Autoclaved Autografts in Mandibular Reconstruction: Case Report and Review of Literature, Journal of Maxillofacial and Oral Surgery 14 (2015) 308-312. doi: 10.1007/s12663-013-0508-5.

[39] K.K. Hallfeldt, H. Stützle, M. Puhlmann, S. Kessler, L. Schweiberer, Sterilization of partially demineralized bone matrix: the effects of different sterilization techniques on osteogenetic properties, The Journal of Surgical Research 5 (1995) 614-620. doi: 10.1006/jsre.1995.1213.

[40] G.F. Draenert, M. Delius, The mechanically stable steam sterilization of bone grafts, Biomaterials 8 (2007) 1531-8. doi:10.1016/j.biomaterials.2006.11.029.

[41] M.J. Sawkins, W. Bowen, P. Dhadda, H. Markides, L.E. Sidney, A.J. Taylor, F.R. Rose, S.F. Badylak, K.M. Shakesheff, L.J. White, Hydrogels derived from demineralized and decellularized bone extracellular matrix, Acta Biomaterialia 8 (2013) 7865–7873. doi: 10.1016/j.actbio.2013.04.029

[42] Y. Su, M. Li, X. Wang, Z. Wang, L. Yi, Denatured Collagen Could Increase the Autophagy Level and Inhibit Apoptosis of Fibroblasts to Help Cell Survival and Influence Wound Healing, the International Journal of Lower Extremity Wounds 10 (2020). doi: 10.1177/1534734620925942.

[43] D. Medhat, C.I. Rodríguez, A. Infante, Immunomodulatory Effects of MSCs in Bone Healing, International Journal of Molecular Sciences 20 (2019) 5467. doi: 10.3390/ijms20215467.

781 [44] A. Dorronsoro, I. Ferrin, J.M. Salcedo, E. Jakobsson, J. Fernández-Rueda, V. Lang, P.
782 Sepulveda, K. Fechter, D. Pennington, C. Trigueros, Human mesenchymal stromal
783 cells modulate T-cell responses through TNF-α-mediated activation of NF-κB,
784 European Journal of Immunology 44 (2014) 480-8. doi: 10.1002/eji.201343668.
785 [45] L.C. Gerstenfeld, T.J. Cho, T. Kon, T. Aizawa, J. Cruceta, B.D. Graves, T.A. Einhorn,
786 Impaired intramembranous bone formation during bone repair in the absence of tumor
787 necrosis factor-alpha signaling, Cells Tissues Organs 169 (2001) 285-94. doi:
788 10.1159/000047893.
789 [46] S. Ivanovski, S. Hamlet, M. Retzepi, I. Wall, N. Donos, Transcriptional profiling of
790 "guided bone regeneration" in a critical-size calvarial defect, Clinical Oral Implants
791 Research 22 (2011) 382-389. doi: 10.1111/j.1600-0501.2010.02104.x.
792 [47] W. Zhang, C. Zhu, Y. Wu, D. Ye, S. Wang, D. Zou, X. Zhang, D.L. Kaplan, X. Jiang,
793 VEGF and BMP-2 promote bone regeneration by facilitating bone marrow stem cell
794 homing and differentiation, European Cells & Materials 27 (2014) 1-11, discussion
795 11-2. doi: 10.22203/ecm.v027a01.
796 [48] Y.B. Shaik-Dasthagirisaheb, G. Varvara, G. Murmura, A. Saggini, G. Potalivo, A.
797 Caraffa, P. Antinolfi, S. Tete, D. Tripodi, F. Conti, E. Cianchetti, E. Toniato, M.
798 Rosati, P. Conti, L. Speranza, A. Pantalone, R. Saggini, T.C. Theoharides, F. Pandolfi,
799 Vascular endothelial growth factor (VEGF), mast cells and inflammation, International
800 Journal of Immunopathology and Pharmacology 26 (2013) 327-35. doi:
801 10.1177/039463201302600206.
802 [49] E. Dohle, I. Bischoff, T. Böse, A. Marsano, A. Banfi, R.E. Unger, C.J. Kirkpatrick,
803 Macrophage-mediated angiogenic activation of outgrowth endothelial cells in co
804 culture with primary osteoblasts, European Cells & Materials 27 (2014) 149-64,
805 discussion 164-5. doi: 10.22203/ecm.v027a12.

806 [50] K. Hu, B.R. Olsen, The roles of vascular endothelial growth factor in bone repair and
807 regeneration, Bone 91 (2016) 30-8. doi: 10.1016/j.bone.2016.06.013.
808

809 **TABLE**

810 **Table 1:** Specific optical rotation value of collagenic fraction extracted from PDBM compared

811 to previous values obtained from collagen coil and collagen helix

812

	Collagen coil at 40°C (2mg/mL)	**Collagen Helix at 27°C (2mg/mL)**	**PDBM at 27°C (1.5mg/mL of collagen-like)**
Specific optical rotation $Deg.cm^{3}.g^{-1}.dm^{-1}$	**-274° +/- 1°**	**-800° +/- 4°**	**-340° +/- 2°**

813

814

815

816 **FIGURE LEGENDS**

817 **Figure 1: Material characterization**

818 Representative light micrographs of the morphology of the PDBM (A) and the BP (D).
819 Representative environmental scanning electron microscopy (eSEM) of the morphology of the
820 PDBM (B-C) and the BP (E-F). Amount of residual DNA (G) in HFH, BP, and PDBM;
821 significant differences are indicated by* ($p<0.05$) (compared to HFH) and # ($p<0.05$)
822 (compared to PDBM). Fourier transform infrared spectrometry (FTIR) (H): absorption spectra
823 of the mineral and the organic phases of BP and PDBM used in the present study. (I)
824 Quantified "collagenic phase" extractible from BP, PDBP, and PDBM.

825

826 **Figure 2. Micro-CT images of the bone healing process within 8-mm-diameter rat**
827 **calvarium defects during the 8 weeks post-surgery.** The calvarium defects tested were
828 either left empty or filled with BP or PDBM paste and were scanned using micro-CT
829 immediately (D0) and 15, 30, 45, and 60 days post-surgery. (A) Representative 2D images
830 illustrating a significant increase (evidenced as radiopacity) in the PDBM paste-filled defects
831 (A3) compared to the BP-filled defects (A2) and the defects left empty (A1). (B) Significant
832 ($p< 0.01$) greater radiopacity volume was present in the PDBM-filled defects compared to the
833 respective results obtained from the BP-filled defects and the defects left empty. Numerical
834 data are shown as means ± SD of 6 samples per animal group. Significant differences are
835 indicated by * $p< 0.05$, and ** $p< 0.01$.

836

837 **Figure 3. Micro-CT follow-up of bone healing within the 4-mm- and 6-mm-diameter rat**
838 **calvarium defects during the 8 weeks post-surgery.** The calvarium defects were either left
839 empty or filled with BP or PDBM paste and were scanned immediately (D0) and 15, 30, 45,
840 and 60 days post-surgery. (A) Representative 2D images illustrating new bone formation in

both the 6-mm- and 4-mm-diameter defects left empty (A1) or filled with BP (A2) or PDBM paste (A3). (B) Radiopacity volume (evidenced as radiopacity) was significantly ($p < 0.01$) greater in the 6-mm PDBM paste-filled defects compared to pertinent results obtained from the BP-filled defects and the defects left empty. (C) Radiopacity volume was similar in the 4-mm-diameter defects that were left empty or filled with the BP and the PDBM paste. Numerical data are shown as means ± SD of 6 samples per animal group. Significant differences are indicated by * $p < 0.05$, and ** $p < 0.01$.

Figure 4. Histology and histomorphometric analyses of new bone formation in the 8-mm-diameter rat calvarium defects at the 8th week post-surgery. (A) and (B) New bone formation (*) in the defects left empty and the BP-filled defects was located at the periphery of the defect. (C) In the PDBM- filled defects, it was present between and around the PDBM particles (p) and in the center of the defect. (D) Magnified light micrograph of the framed section in Figure 4C illustrates new bone formation (*) in contact with PDBM particles (p), osteoblasts (white arrow), and osteocyte lacunas (blue arrow). (E) The area of the new bone formation in the defects filled with the PDBM paste was significantly higher ($p < 0.001$) than those obtained from the BP-filled defects and the defects left empty. **Stains:** Stevenel's blue and Van Gieson picro fuschin were used for the visualization of cell nuclei and bone tissue, respectively. Significant difference ($p < 0.01$) is indicated by ****.**

Figure 5. Histology and histomorphometric analyses of new bone formation in 6-mm-diameter rat calvarium defects at the 8th week post-surgery. (A) and (B) New bone formation (*) in the 6-mm-diameter defects left empty or filled with the BP was located at the edge and inside the defects. (C) Bone formation (*) in the defects filled with the PDBM paste was present between and around the PDBM paste particles (p) and in the center of the defects.

(D) Magnified light micrograph of the framed section in Figure 5C illustrates histology details such as woven bone in contact with the residual PDBM particles. Osteocyte-like and some lining cells, as well as blood vessels were observed in the bone marrow spaces. * = newly-formed bone; P = PDBM paste; MO = bone marrow; Dotted line = edge of the defect; Arrow points to an osteocyte lacuna; Ob = osteoblast.(E) Quantitative analysis showed significantly a wider area of new bone formation in the defects filled with PDBM compared to those that had been left empty or filled with the BP. Significant difference ($p < 0.05$) is indicated by *.

Figure 6. Histology and histomorphometric analyses of new bone formation in 4-mm-diameter rat calvarium defects at the 8th week post-surgery. An important new bone formation (*) was observed in the 4-mm-diameter defects which had been left empty (A) or filled with BP (B). In the defects filled with PDBM paste (C), bone formation (*) was observed between and around the PDBM particles (p) and in the center of the defect. (D) The new bone formation was similar in the empty defects and in the BP- or PDBM paste-filled defects.

Figure 7. Time course of selected inflammation- and angiogenesis-related genes' expression levels in the 8-mm-diameter bone defects on days 3, 7, and 14 post-surgery. The defects had been left empty (white columns) or filled with PDBM (black columns). The basis of comparison for the observed significant differences ($p < 0.05$) are the following lower case letters: a = significant difference from pertinent results obtained for empty defect group; b = significant difference compared to the results obtained from PDBM group; c = significant difference compared to the results obtained for the same gene in the same group on D3; d = significant difference compared to the results obtained for the same gene in the same group on D14. TNFα = Tumor necrosis factor; IL-1β = Interleukin 1β; IL-6 = Interleukin 6; IL-8 =

891 Interleukin 8; VEGF = Vascular endothelial growth factor; ANG = Angiogenin; CDH5 =
892 Cadherin 5; PECAM1 = Platelet endothelial cell adhesion molecule; VWF= Von Willebrand
893 factor.

894 **Figure 8: Time course of expression of selected genes related to bone formation and**
895 **remodeling in the 8-mm-diameter bone defects on days 3, 7, and 14 post-surgery.** The
896 defects had been either left empty (white columns) or filled with PDBM (black columns).
897 Statistically significant differences ($p < 0.05$) are indicated by the following lower case letters:
898 a = significant difference from pertinent results obtained for empty defect group; b =
899 significant difference compared to the results obtained from PDBM group; c = significant
900 difference compared to the results obtained for the same gene in the same group on D3; d =
901 significant difference compared to the results obtained for the same gene in the same group on
902 D14. ALP = Alkaline phosphatase; RUNX2 = Runt-related transcription factor 2; COL1A1 =
903 alpha-1 type I Collagen; BGLAP (Osteocalcin) = Bone gamma-carboxyglutamate protein; SP7
904 = Transcription factor Sp7 or Osterix (Osx); MMP13 = Matrix metalloproteinase 13; OPG =
905 Osteoprotegerin; RANKL = Receptor activator of nuclear factor kappa-B ligand; SPARC
906 (Osteonectin) = Secreted protein acidic and rich in cysteine.
907

Table 1: specific optical rotation value of collagenic fraction extracted from PDBM compared to previously values observed from collagen coil and collagen helix

	Collagen coil at 40°C (2mg/ml)	Collagen Helix at 27°C (2mg/ml)	PDBM at 27°C (1,5mg/ml of collagen-like)
Specific optical rotation $Deg.cm^3.g^{-1}.dm^{-1}$	-274° +/- 1°	-800° +/- 4°	-340° +/- 2°

Figure 1. Material characterization

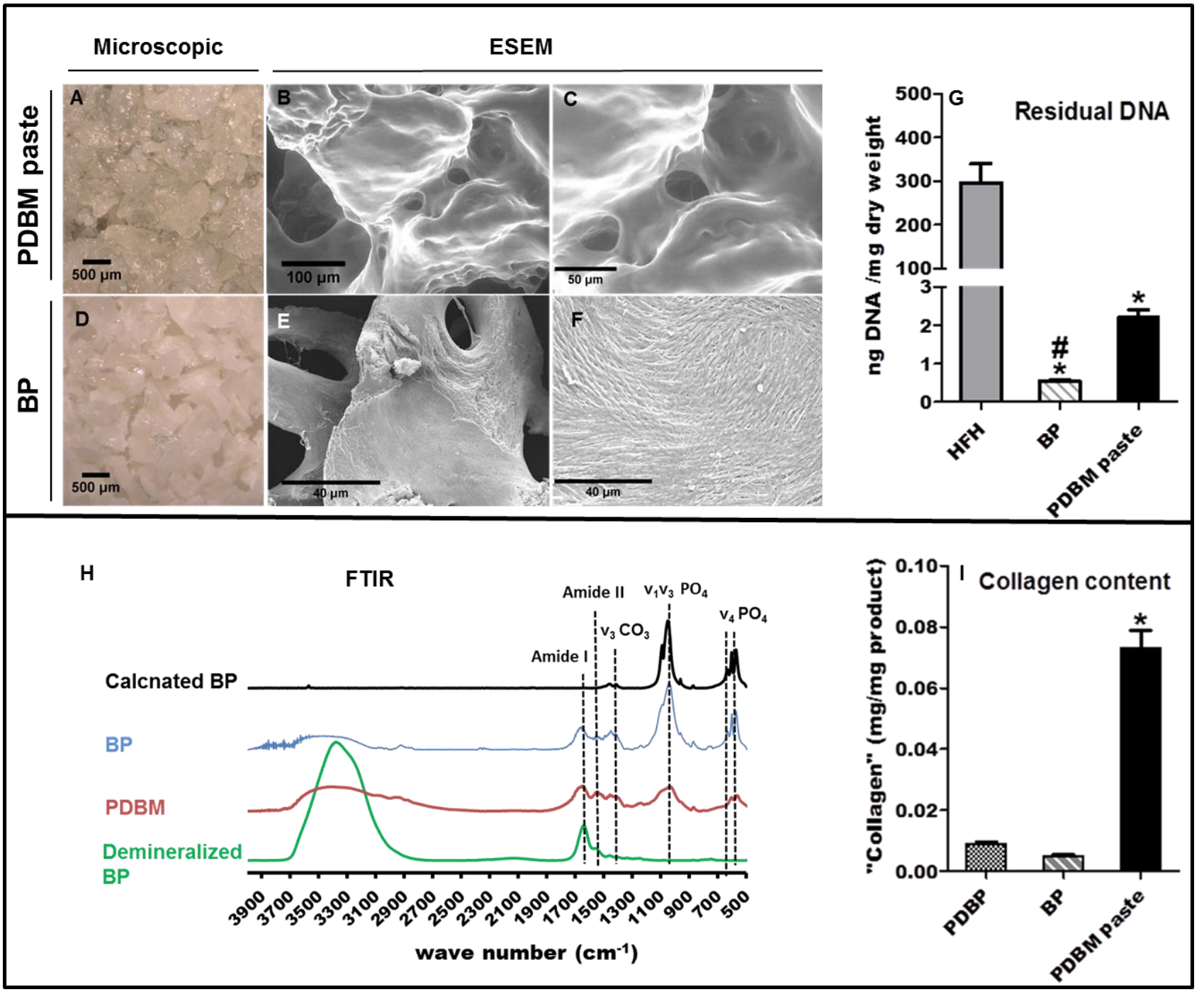

Figure 2. Micro-CT images of the bone repair process within 8-mm-diameter rat calvarium defects during 8 weeks post-surgery.

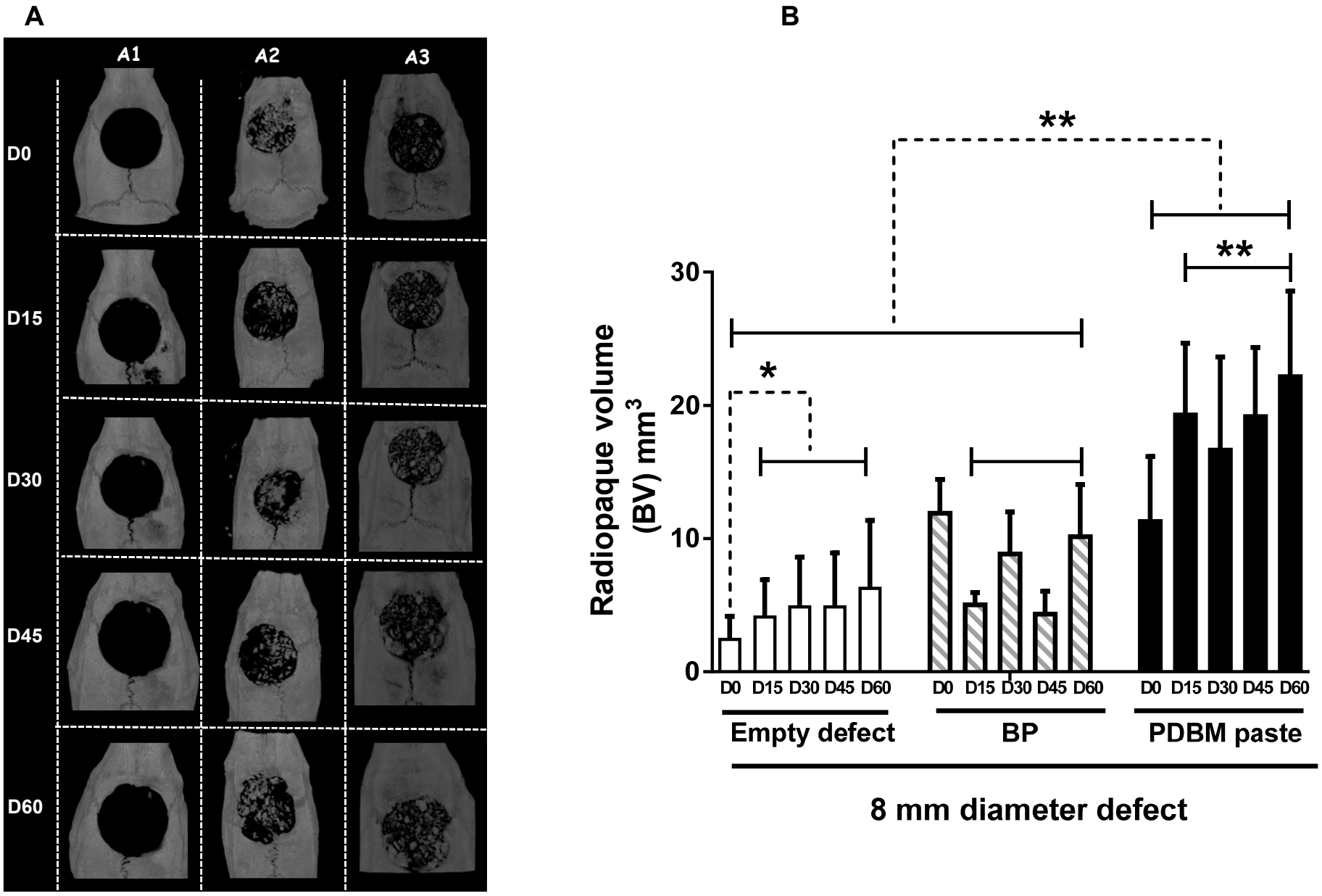

Figure 3. Micro-CT follow-up of bone repair within the 4-mm- and 6-mm-diameter rat calvarium defects during 8 weeks post surgery.

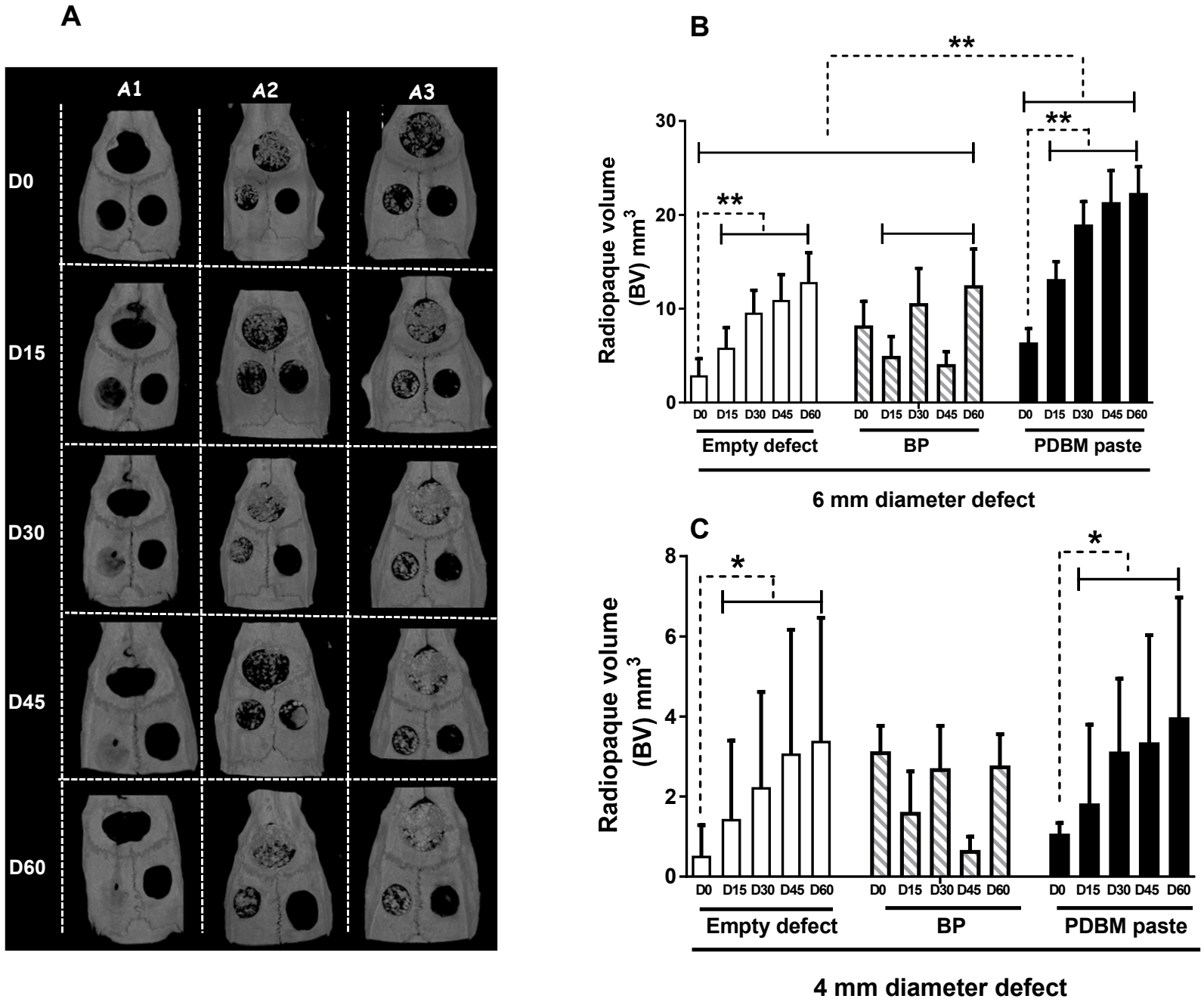

Figure 4. Histology and histomorphometrical analysis of new-bone formation in the 8-mm-diameter rat calvarium defects at the 8th weeks post-surgery.

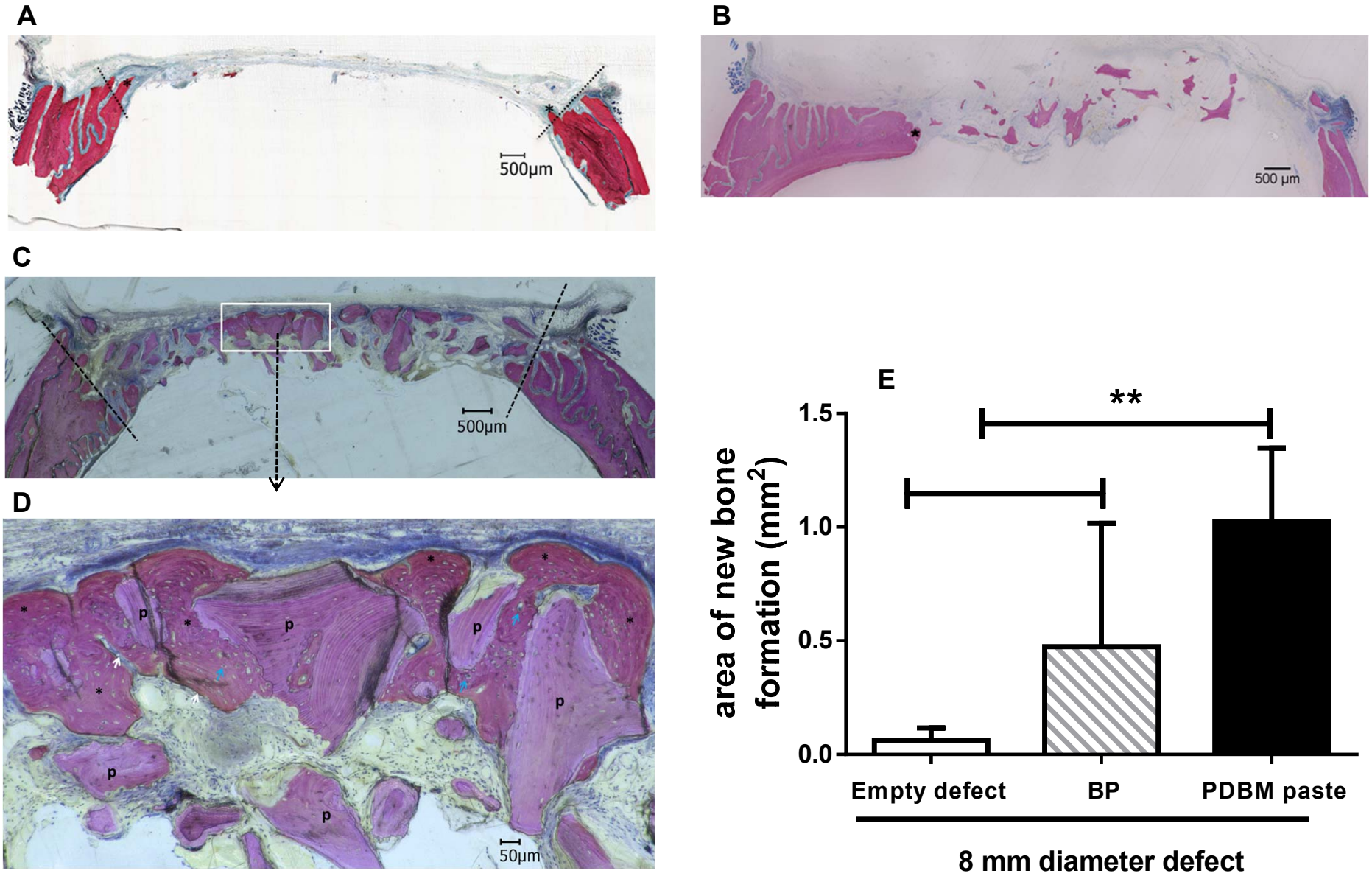

Figure 5. Histology and histomorphometrical analyses of new-bone formation in 6-mm-diameter rat calvarium defects at the 8th week post-surgery.

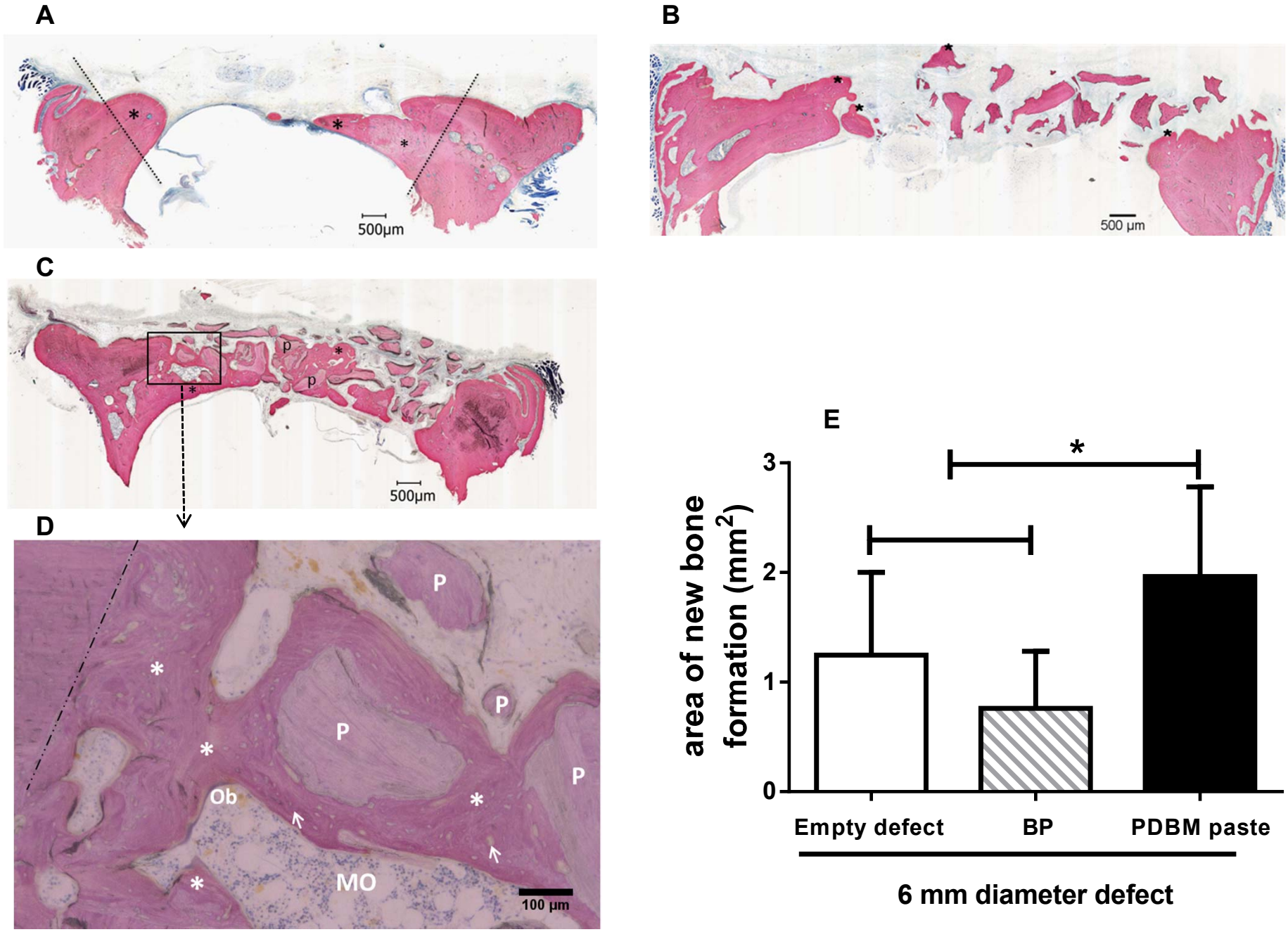

Figure 6. Histology and histomorphometrical analyses of new bone formation in 4-mm-diameter rat calvarium defects at the 8th week post-surgery.

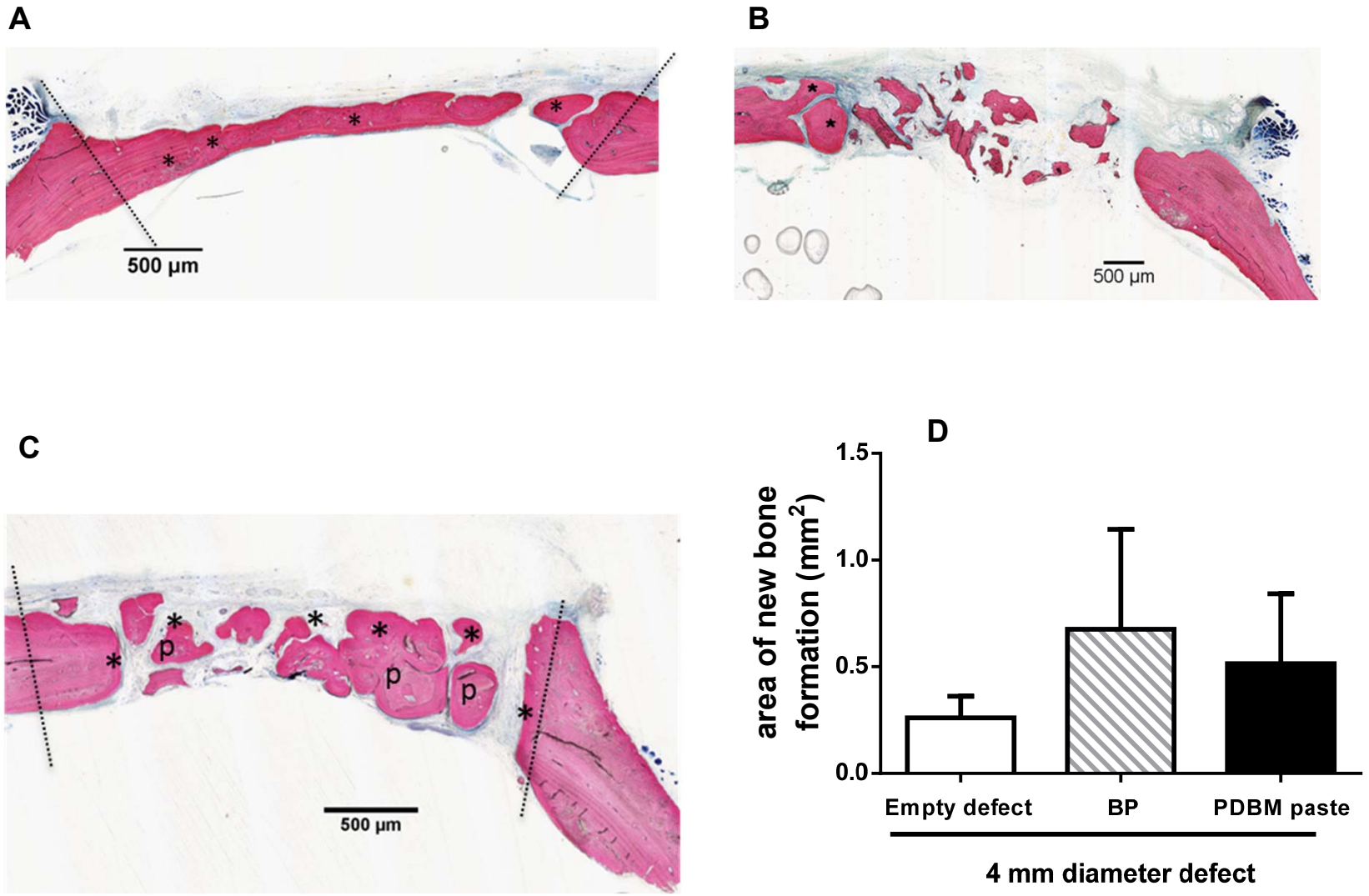

Figure 7: Gene expression analysis of pro-inflammatory and angiogenesis markers in the 8-mm diameter bone defects after 3, 7 and 14 days of healing.

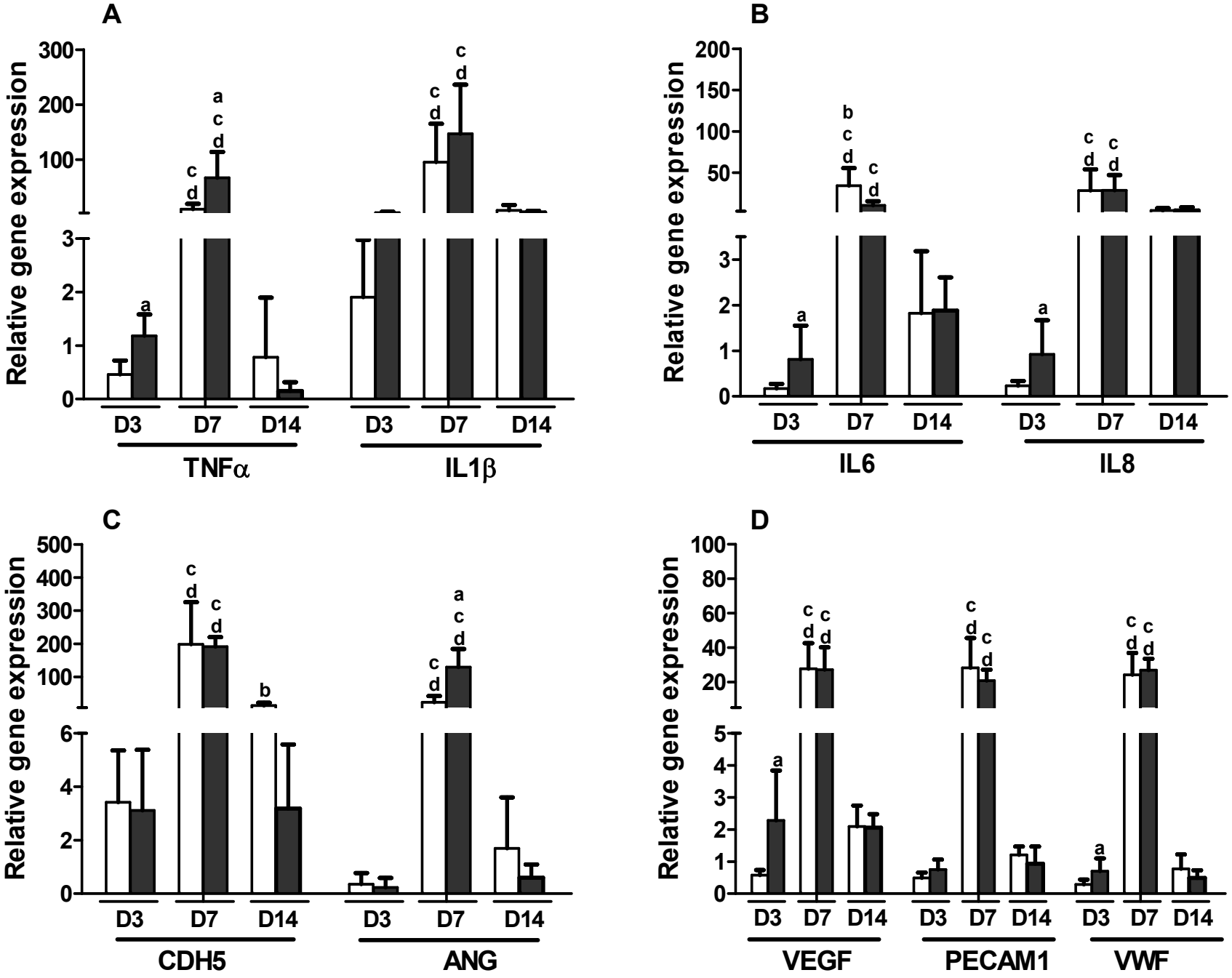

Figure 8: Gene expression analysis of bone formation and bone resorption markers, in the 8-mm diameter bone defects after 3, 7 and 14 days of healing.